

Article

Ground Return Current Behaviour in High Voltage Alternating Current Insulated Cables

Roberto Benato ^{1,*}, **Sebastian Dambone Sessa** ¹, **Fabio Guglielmi** ¹, **Ertugrul Partal** ²
and **Nasser Tleis** ³

¹ Department of Industrial Engineering, University of Padova, Via Gradenigo, 6/A, Padova 35131, Italy; E-Mails: sebastian.dambonesessa@unipd.it (S.D.S.); fabio.guglielmi@unipd.it (F.G.)

² National Grid Electricity Transmission, Gallows Hill, Warwick CV34 6DA, UK;
E-Mail: ertugrul.partal@nationalgrid.com

³ Power & Water Planning Division, P.O. Box 564, Dubai, UAE; E-Mail: nasser.tleis@dewa.gov.ae

* Author to whom correspondence should be addressed; E-Mail: roberto.benato@unipd.it;
Tel.: +39-049-8277-532; Fax: +39-049-8277-599.

External Editor: Paul Stewart

Received: 23 September 2014; in revised form: 20 November 2014 / Accepted: 25 November 2014 /
Published: 3 December 2014

Abstract: The knowledge of ground return current in fault occurrence plays a key role in the dimensioning of the earthing grid of substations and of cable sealing end compounds, in the computation of rise of earth potential at substation sites and in electromagnetic interference (EMI) on neighbouring parallel metallic conductors (pipes, handrails, etc.). Moreover, the ground return current evaluation is also important in steady-state regime since this stray current can be responsible for EMI and also for alternating current (AC) corrosion. In fault situations and under some assumptions, the ground return current value at a substation site can be computed by means of k -factors. The paper shows that these simplified and approximated approaches have a lot of limitations and only multiconductor analysis can show the ground return current behaviour along the cable (not only the two end values) both in steady-state regime and in short circuit occurrence (e.g., phase-to-ground and phase-to-phase-to-ground). Multiconductor cell analysis (MCA) considers the cable system in its real asymmetry without simplified and approximated hypotheses. The sensitivity of ground return current on circuit parameters (cross-bonding box resistances, substation earthing resistances, soil resistivity) is presented in the paper.

Keywords: ground return current; insulated cables; multiconductor cell analysis; asymmetric systems

1. Introduction

Undergrounding electrical power is and will be more and more in the future an unavoidable and paramount issue for the development and reinforcement of extra high voltage (EHV) electric grid. Whereas there are numerous contributions in technical literature concerning the ground return current in overhead lines (OHL), the same issue for underground insulated cables (UGC) does not seem to have been investigated other than for cross-bonded EHV UGC. The paper deals with this topic. The use of multiconductor cell analysis (MCA) (implemented in MATLAB environment) for asymmetric power systems has been already presented with reference to:

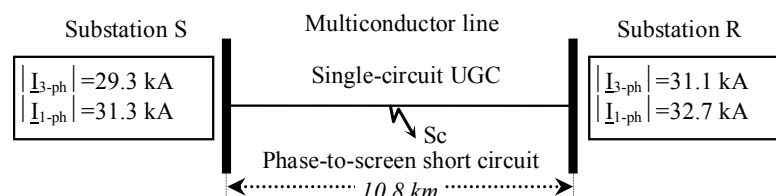
- EHV overhead lines with any number of earth wires [1];
- Milliken conductors [2];
- Harmonic behaviour of high voltage direct current (HVDC) cables [3];
- Distribution line carrier (DLC) in medium voltage (MV) network [4];
- Alternating current (AC) gas Insulated transmission Lines (GILs) [5];
- AC high-speed railway supply [6].

In particular, the application of MCA to AC EHV UGC has been reported in [7]. When the aim is the computation of the rise of earth potential (ROEP) at substation sites there are several contributions in the literatures involving the k -factors [8–21]. These contributions are generally based on solidly-bonded (SB) cables and are not applicable to cross-bonded cables. Solid bonding is a usual screen arrangement for low voltage (LV) and MV insulated cables and short high voltage (HV) and EHV cables used as substation entry connections. Otherwise, cross-bonded HV and EHV cables are used. Extensive comparisons between MCA and ElectroMagnetic Transient Program-Restructured Version (EMTP-RV) have shown a very good agreement. The computation of the short circuit current by means of sequence theory is also presented.

2. Fault Occurrence in a Cross-Bonded Single Circuit Cable Line by Means of Multiconductor Cell Analysis

The first situation to be investigated is depicted in Figure 1. The single-circuit cross-bonded (CB) with phase transpositions (PTs) UGC is supplied at both ends. The fault levels (sub-transient three-phase and single-phase short circuit currents) are shown in the same figure (true values of Great Britain nodes).

Figure 1. Single-circuit faulted underground insulated cables (UGC) supplied at both ends.

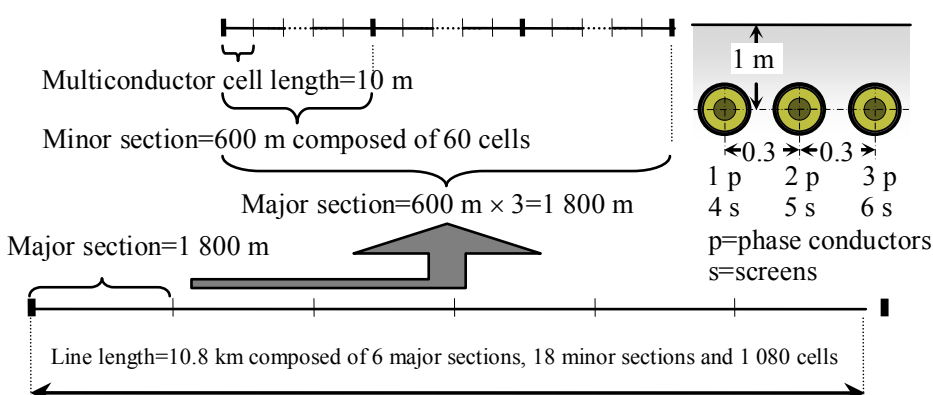


Let us suppose a phase-to-screen short circuit at the UGC midline (*i.e.*, 5.4 km from sending and receiving ends with UGC length = 10.8 km). The UGC characteristics are reported in Table 1 and the MCA model in Figure 2. It is worth remembering that, after IEC 60909-0 [22], the phase conductor must be computed at 20 °C (so that also the proximity and skin effect parameters y_s and y_p must be computed at 20 °C). The use of PTs has been chosen in tune with the Great Britain installation but MCA can consider also un-transposed cable lines.

Table 1. Geometric and electric data of XLPE-insulated single-core cable. XLPE: cross-linked polyethylene; PE: polyethylene; CB: cross-bonding.

Cable type insulation	Unit	XLPE
Voltage levels after IEC 62067	kV	220/380 (420)
Cross sectional area/material	mm ²	2500/Cu M-type
Conductor diameter	mm	64.3
Conductor screen diameter d_0	mm	68.7
Insulation diameter d_1	mm	122.8
Insulation screen diameter	mm	126.1
Metallic shield diameter/material	mm	131.3/Al welded
Jacket of PE diameter	mm	142.4
Overall diameter	mm	142.4
Per unit length 50 Hz resistance of phase conductor at 20 °C	mΩ/km	8.4827
Per unit length series Inductance	mH/km	0.5431
Per unit length shunt Leakance (50 Hz) with loss factor $\tan\delta = 0.0007$	nS/km	48.4
Per unit length shunt Capacitance with $\epsilon_r = 2.3$	μF/km	0.22
Per unit length zero sequence impedance z_0	Ω/km	0.0547 + $j \cdot 0.0612$
Line length	km	10.8
Cell length	m	10
Earth resistivity	Ω·m	100
Substation earthing resistances R_A and R_B	Ω	0.1
Major section CB box resistance R	Ω	5
Link resistance R_{cont} between screens at earthing sites	mΩ	1

Figure 2. Subdivision of the single-circuit cable line in cross-bonding with indication of cells and minor and major sections (not to scale).



The phase 2—screen 5 short circuit (at 5.4 km from sending and receiving ends) current is equal to:

$$I_{1P} = -51.5 + j28 \text{ kA} = 58.6 \text{ kA} \angle 151.5^\circ$$

The short circuit current returns equally (see Figure 3; the value is about 9.82 kA) in all the screens due to the presence of CB; but at any intermediate screen bonding and earthing point, it slightly decreases since there is an injection into the earth; consequently the ground return current of Figure 4 obviously increases at the same locations. The ground return current is rather high (maximum 1.65 kA) since, as it will be demonstrated, the CB box resistances are low (equal to 5 Ω as in Table 1). In the following the dependence of $|I_{GR}|$ upon this parameter is also shown.

Figure 3. Faulted UGC: screen current magnitudes along the line CB with phase transpositions (PTs); FAULT at midline.

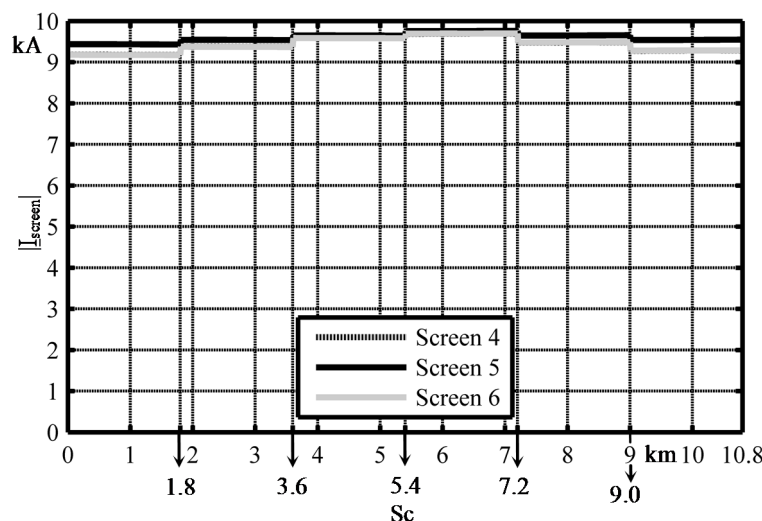
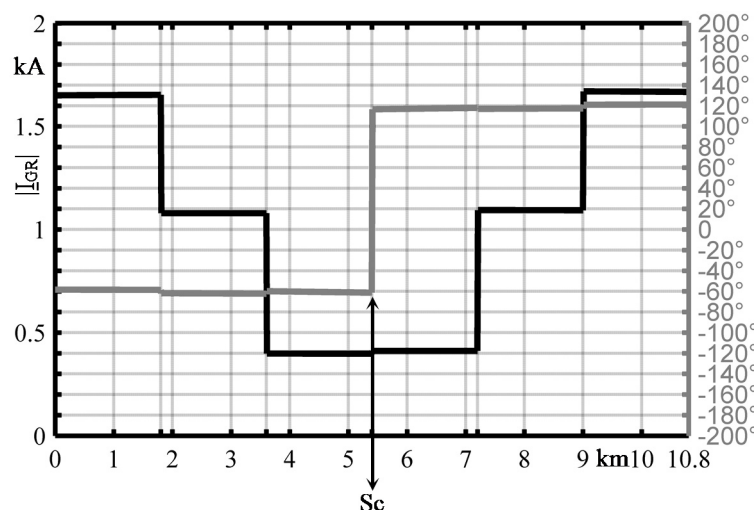


Figure 4. Faulted UGC: ground return current magnitude and angle along the line (CB with PTs); FAULT at midline.



The case of CB without PTs has no great differences with the case of CB with PTs and it is not reported. In order to understand the sensitivity of $|I_{GR}|$ on the circuit parameters and the fault locations the following Figures 5–9 are very helpful.

Figure 5. Faulted UGC: ground return current magnitudes along the line (CB with PTs) for different CB box resistances; FAULT at midline.

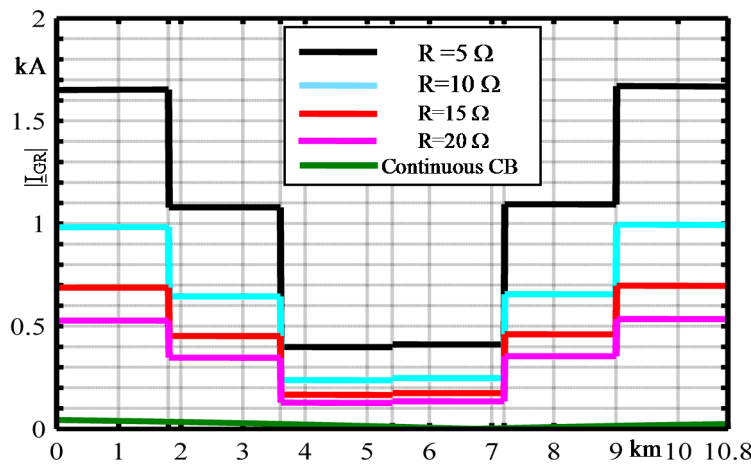


Figure 6. Faulted UGC: ground return current magnitudes along the line (CB with PTs) for different earth resistivities; FAULT at midline.

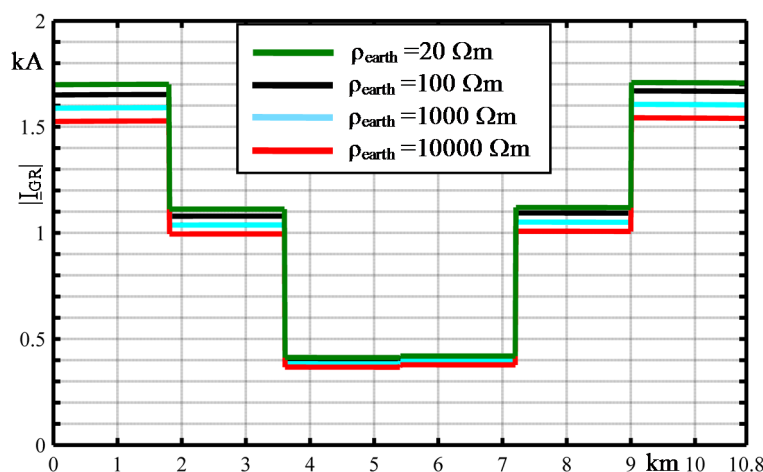


Figure 7. Faulted UGC: ground return current magnitudes along the line (CB with PTs) for different substation grid resistances; FAULT at midline.

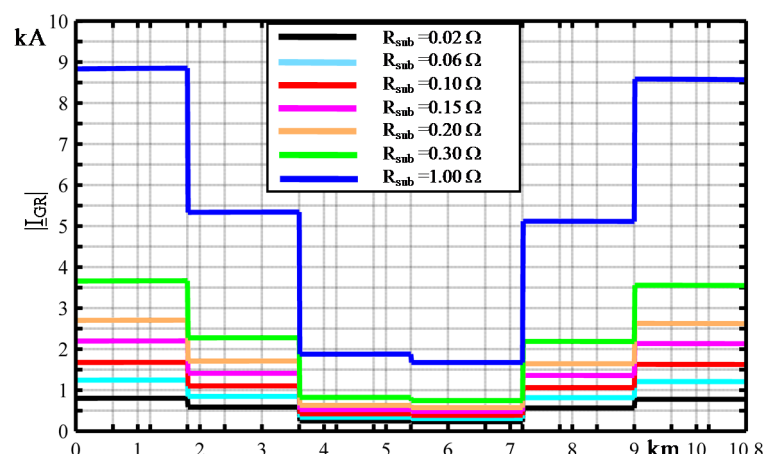


Figure 8. Faulted UGC: ground return current magnitudes along the line (CB with PTs) for different fault locations.

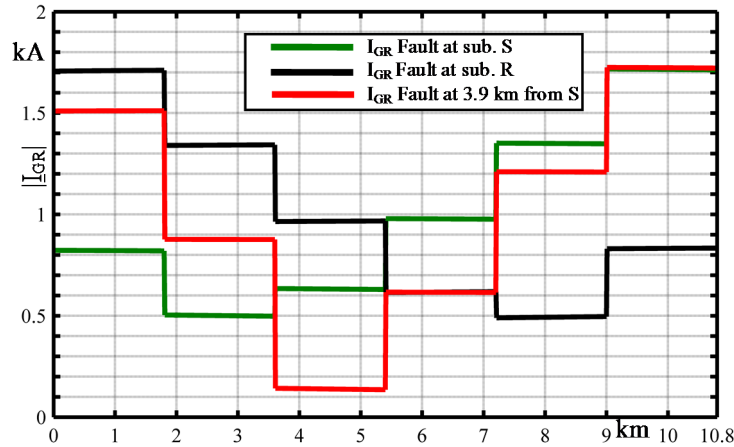


Figure 9. Double-circuit UGC (CB with PTs) in electrical parallel.

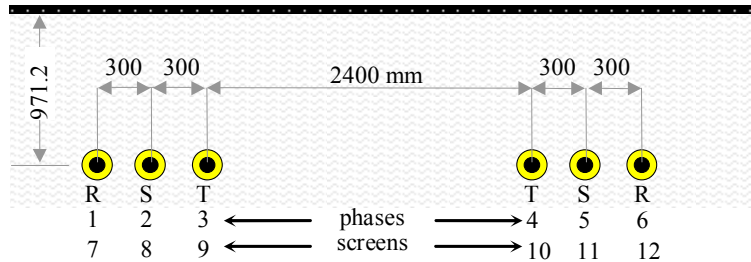


Figure 5 compares five ground return current magnitudes for five different values of CB box resistance (*i.e.*, $R = 5, 10, 15, 20, 1 \times 10^9 \Omega$). If the CB box resistance is high (*e.g.*, $R = 20 \Omega$) the ground return current decreases meaningfully (it reduces from 1.65 kA to 0.5 kA of Figure 5). The sharing of fault current in the screens is rather unaffected by the CB box resistances but, of course, with lower ground return current there are higher current in the screens. Therefore, it is demonstrated that an important role is played by the CB box resistances (at major section location) which are responsible for the injection of current into the earth and hence for the creation of $|I_{GR}|$.

The last value of $R = 1 \text{ G}\Omega$ is meaningful for the continuous CB namely, in the CB boxes (at major section locations), the screens are not bonded and not earthed. This can be easily accounted for in the MCA, by setting $R \rightarrow \infty$ (it is sufficient to set $R = 1 \text{ G}\Omega$ and contact resistances [7] $R_{\text{cont}} = 1 \text{ G}\Omega$). It is not a theoretical case since it has been employed in the St. Johns Wood-Elstree UGC [23,24]: a 20 km long 400 kV cross-linked polyethylene (XLPE)-insulated cable system. In this UGC, the continuous cross-bonding method has been employed since it is a tunnel installation [25] and could not use a distributed earthing system inside the tunnel. This practice is very convenient for ground return current (since CB becomes a kind of SB with the differences that the screens are transposed) but not for screen induced voltages since there are not locations along the line where the screens are linked to the earth anymore (but at the substation locations). The sensitivity of ground return current on the soil resistivity is less important than that on CB box resistances.

Figure 6 shows the different ground return current magnitudes for $\rho_{\text{earth}} = 20 \Omega \cdot \text{m}$, $100 \Omega \cdot \text{m}$, $1000 \Omega \cdot \text{m}$ and $10000 \Omega \cdot \text{m}$ unchanged with the CB box resistances = 5Ω . It is worth noting that

$\rho_{\text{earth}} = 20 \Omega \cdot \text{m}$ is representative of British soil conditions for the vast majority of locations. All the above mentioned results are based on the assumption that the two earthing grid substation resistances are equal to 0.1Ω . This is rather reasonable for an EHV substation. A range where this resistance can change is about $0.02 \div 0.3 \Omega$ depending upon the substation extension and the earth resistivity. The ground return current is extremely sensitive to the substation grid resistances which are mostly responsible for the screen voltage behaviour. The higher is the substation grid resistances the more the screens are “floating”. Since the line length is not great, the substation grid resistances (together with the lumped resistances of CB boxes) play a key role in the I_{GR} . In order to understand this influence, in Figure 7, by fixing the values of CB box resistances (*i.e.*, 5Ω), different ground return current magnitude behaviours are shown (for a midline short circuit between phase 2 and screen 5) with different substation grid resistances from $R_{\text{sub}} = 0.02 \Omega$ to $R_{\text{sub}} = 1.00 \Omega$.

The above presented cases deal with phase 2-screen 5 short circuit at midline. If the short circuit occurs at different locations along the line, $|I_{GR}|$ behaviour changes very slightly. In order to confirm it, Figure 8 shows $|I_{GR}|$ behaviour for three short-circuit locations:

- i. at S substation;
 - ii. at R substation;
 - iii. at 3.9 km from S substation.

Other types of short circuit are not considered in this paper (e.g., phase-to-phase-to-ground short circuit) since, along the line, the only (and more probable) short circuit is the phase-to-screen one.

Ground Return Current in Double Circuit Underground Cable

When a double-circuit UGC in electrical parallel is employed (Figure 9), $|I_{GR}|$ behaviour, during a short circuit on a faulted circuit, lessens due to the presence of the unfaulted circuit screens. Figure 10 shows the sharing of short circuit current magnitude on the different screens: the unfaulted circuit screens subtract current to the ground. This is confirmed by the comparison of $|I_{GR}|$ in Figure 4 with that of Figure 11. Ground return current for two different fault locations is shown in Figure 12.

Figure 10. Faulted double-circuit UGC: screen current magnitudes along the line (CB with PTs); FAULT at midline.

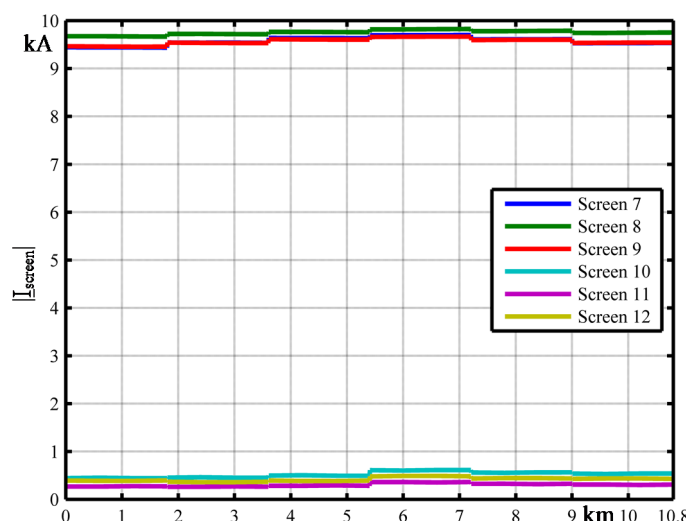


Figure 11. Faulted double-circuit UGC: ground return current magnitudes along the line (CB with PTs); FAULT at midline.

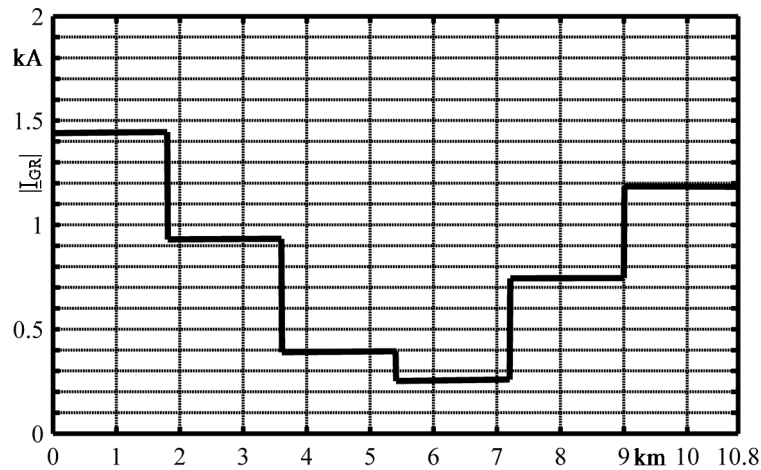
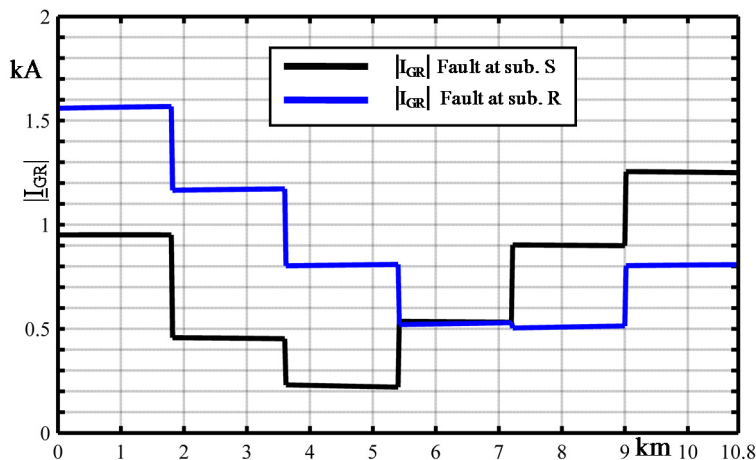


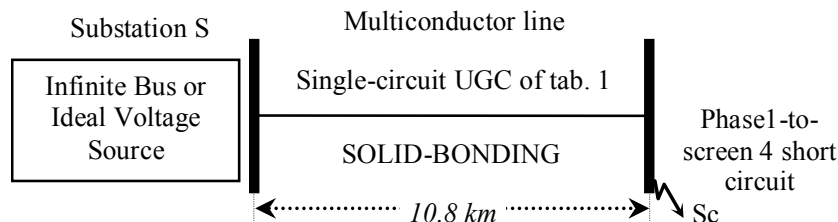
Figure 12. Faulted double-circuit UGC: ground return current magnitudes along the line (CB with PTs) for two different locations.



3. Comparison with *k*-Factors

In this section a comparison between MCA and *k*-factor approaches found in technical literature [8–19] and international standards [20,21] is presented. Figure 13 shows a single-circuit solid-bonded UGC during a phase 1-to-screen 4 short circuit: it occurs at receiving-end. The circuit is fed by an ideal three-phase voltage source, and it is open-circuited at receiving-end.

Figure 13. Faulted single-circuit UGC supplied at sending end.



It is worth remembering that the k -factor is defined as:

$$\underline{k} = \frac{I_{\text{GR (at sending-end substation)}}}{I_{\text{1P (at fault location)}}} \quad (1)$$

In this case three analytical expressions [17,20] are used for k -factor computations:

$$\underline{k} = \frac{(Z_{\text{cls1}} - Z_{\text{ss}})(Z_{\text{s1s2}} - Z_{\text{ss}})}{Z_{\text{ss}}^2 - 2Z_{\text{s1s2}}^2 + Z_{\text{ss}}Z_{\text{s1s3}} + (3Z_{\text{ss}} + Z_{\text{s1s3}} - 4Z_{\text{s1s2}}) \cdot \left(\frac{R_A + R_B}{L} \right)} \quad (2)$$

$$\underline{k} = \frac{(Z_{\text{cls1}} - Z_{\text{ss}})(Z_{\text{s1s2}} - Z_{\text{ss}})}{Z_{\text{ss}}^2 - 2Z_{\text{s1s2}}^2 + Z_{\text{ss}}Z_{\text{s1s3}}} \quad (3)$$

$$\underline{k} = \frac{R_s}{R_s + 3\omega \frac{\mu_0}{8} + j3\omega \frac{\mu_0}{2\pi} \ln \frac{\delta}{\sqrt[3]{r_{\text{sm}} \cdot d_{12} \cdot d_{13}}}} \quad (4)$$

where Z_{ss} = self-impedance of screen, Z_{cls1} = mutual impedance between phase conductor and screen, Z_{s1s2} = mutual impedance between two adjacent cables, Z_{s1s3} = mutual impedance between outer cables. These impedances can be easily computed by means of Carson-Clem formulae [7]. Substation resistances are not considered in Equation (3) whereas in Equation (2) they can be accounted for. Equation (4) is given by IEC 60909-2 [20] (and IEC 60909-3 [21]) for cables in trefoil arrangement, where R_s = resistance of metallic screen (Ω/km), $\mu_0 = 4\pi \cdot 10^{-4}$ (H/km), $r_{\text{sm}} = 0.5(r_{\text{s_in}} + r_{\text{s_out}})$ (m), d_{12} = distance between adjacent cables (m), d_{13} = distance between outer cables (m).

IEC 60909-3 [21] states that the result found from Equation (4) is the exact result for a triangular configuration. For a flat configuration the result of Equation (4) can be used as a sufficient approximation for this standard, independently if the line-to-earth short-circuit current will occur in an outer cable or the central cable of the flat configuration.

By using Equation (4) of IEC, it yields:

$$\underline{k} = 0.0036 - j0.0292 \Rightarrow |\underline{k}| = 0.0294$$

$$\underline{k} = 0.0063 - j0.0326 \Rightarrow |\underline{k}| = 0.033203$$

so that the agreement is extremely good with Equations (2) and (3) in the literature, but not with IEC Equation (4) (which underestimates the ground return current by 11.5%). Each reader can evaluate if the IEC approximation provides sufficient accuracy for the intended application.

It has been shown that in trefoil arrangement the agreement between literature formulae and MCA is excellent. Moreover, it has been verified with MCA that the behaviour of ground return current during phase 1-to-screen 4 short circuit is constant along the line. If the short circuit location is along the line at ℓ distance from sending-end, the paper [8] gives this general formula:

$$\underline{k}_{\text{along line}} = \frac{\ell}{L} \underline{k} \quad (5)$$

where ℓ is the distance between sending-end and fault location and L is the cable length.

By comparing MCA and k -factor for the last situation (short circuit along the line) it is confirmed a whole agreement (Table 2).

Table 2. Comparison between multiconductor cell analysis (MCA) and k -factor for short circuit along the line A.

Short circuit location	$ k L.M. Popović$	$ k MCA$
$\ell = \frac{1}{4}L$	0.0083	0.0082
$\ell = \frac{1}{2}L$	0.0166	0.0165
$\ell = \frac{3}{4}L$	0.0249	0.0248

3.1. Cross-Bonded Cable

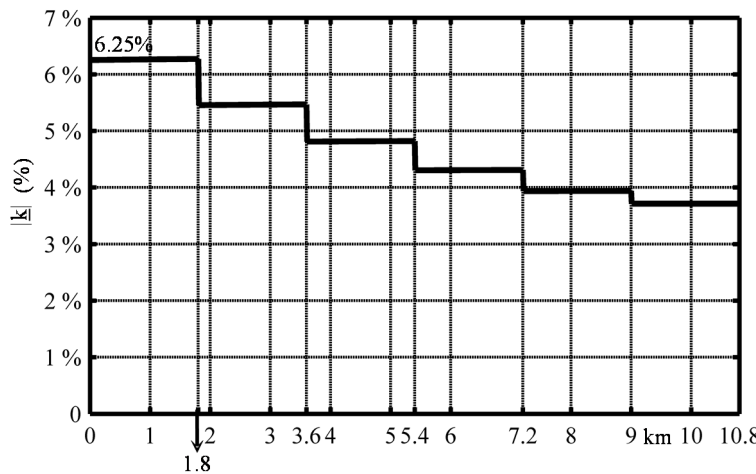
It is worth noting that applying the k -factors derived for solidly-bonded cables to cross-bonding cables is not valid and produces an underestimate. By replacing the cables of Figure 13 with a cross-bonded cable and by means of MCA, Figure 14 shows the magnitude of the following ratio:

$$|k| = \left| \frac{I_{GR}}{I_{1P(\text{at fault location})}} \right| \cdot 100$$

i.e., the percent ratio between the behaviour of $|I_{GR}|$ along the line and the short circuit current $|I_{1P}|$ at fault location.

By using Equation (1) in MCA it yields $|k| = 6.25\%$ (this is the first point of the curve in Figure 14). Without the phase transpositions the k -factor slightly increases, i.e., $|k| = 6.59\%$. This is almost twice of $|k| = 3.32\%$ computed from equations derived for solidly bonded cables. Clearly, these equations are not applicable to CB (with or without phase transposition) UGC.

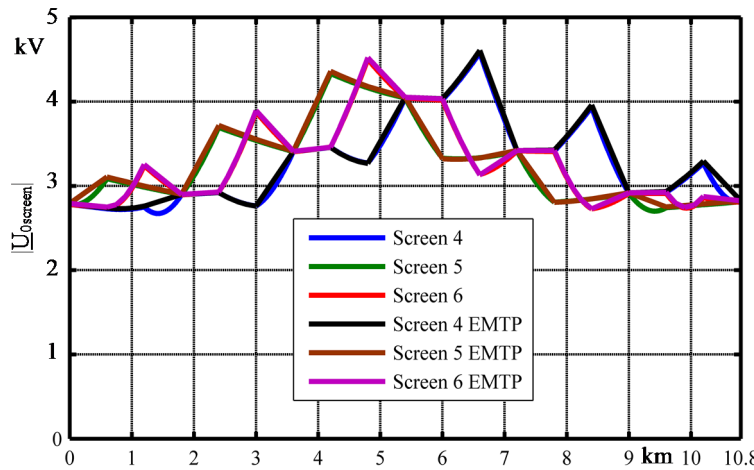
Figure 14. Behaviour of the k -factor percentage along the line by means of MCA.



4. Comparison with ElectroMagnetic Transient Program-Restructured Version

With reference to the configuration of Figure 1, all the MCA results have been extensively validated by EMTP-RV comparisons. In the following a brief report of this comparison is shown. In Figure 15, the screen voltage magnitudes under phase-to-screen short circuit at midline calculated by means of MCA and EMTP-RV are compared.

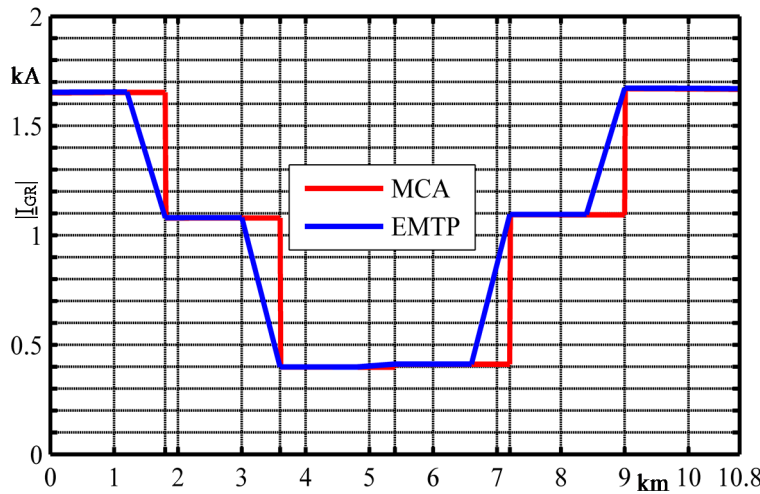
Figure 15. Screen voltage magnitudes comparison between MCA and ElectroMagnetic Transient Program-Restructured Version (EMTP-RV) under phase-to-screen short circuit in a single circuit UGC.



The maximum percentage difference in the screen voltage magnitudes between the MCA and EMTP-RV is less than 0.3%. Similarly, for the two methods, the maximum percentage difference in screen currents is less than 0.05%, *i.e.*, practically zero.

In Figure 16, the comparison between ground return current behaviours is shown. The differences between MCA and EMTP-RV behaviours are only due to the different lengths of EMTP-RV (150 m) and MCA (10 m) cells. If the same MCA cell length is assumed in EMTP-RV, the results are almost equal.

Figure 16. $|I_{GR}|$ under phase-to-screen short circuit in a single circuit UGC.



In conclusion, the difference between the results obtained by means of EMTP-RV and those by means of MCA is negligible (<0.5%).

5. Comparison with Sequence Theory

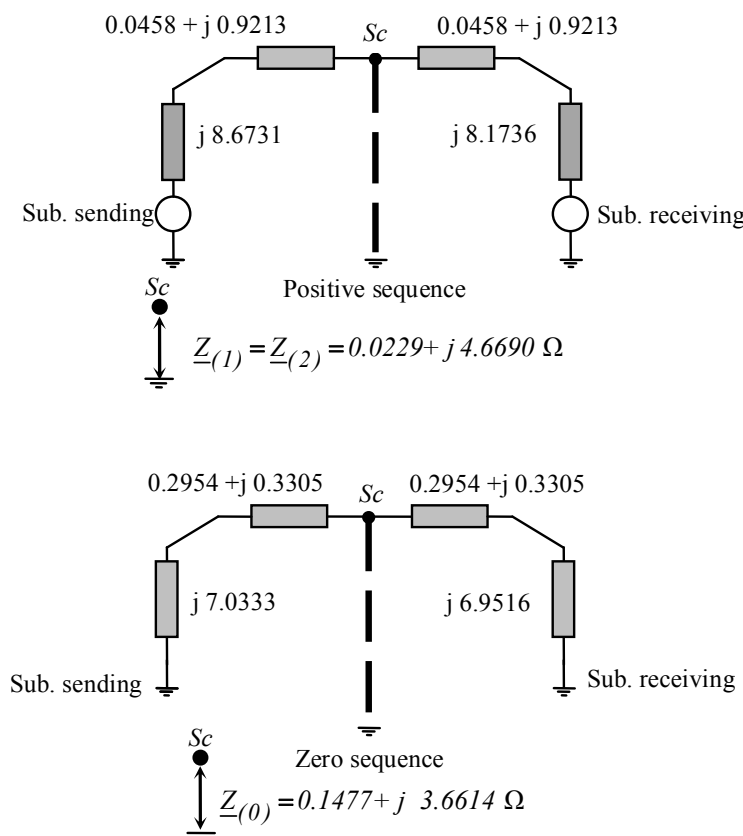
In this section a comparison with the sequence theory is performed since it could be a helpful tool for readers. Of course, this approach is valid only for symmetric lines and UGC has always a given degree

of asymmetry (almost negligible if CB with PTs is performed). However, only in order to have an idea of the errors by considering the line as a perfectly symmetric one, it is possible to compute the UGC sequence impedances (SI). The scheme to be considered is shown in Figure 17 for the positive (negative) and zero sequences respectively. With regard to the UGC impedances, the positive-negative and zero sequence kilometric impedances have been already computed (Table 1) and their values as seen from the fault location are reported in Figure 17. The single-phase short circuit current is given by:

$$\underline{I}_{IP} = \frac{c \cdot 3 \cdot U_0}{\underline{Z}_{(1)} + \underline{Z}_{(2)} + \underline{Z}_{(0)}} = \frac{c \cdot 3 \cdot 400000}{\sqrt{3} \cdot (0.1935 + j \cdot 12.9994)} = 58.620 \text{ kA} \angle -89.147^\circ$$

where c is equal to 1.1 according to IEC 60909-1.

Figure 17. Faulted UGC: positive and zero sequence circuit for single-phase short circuit at midline.



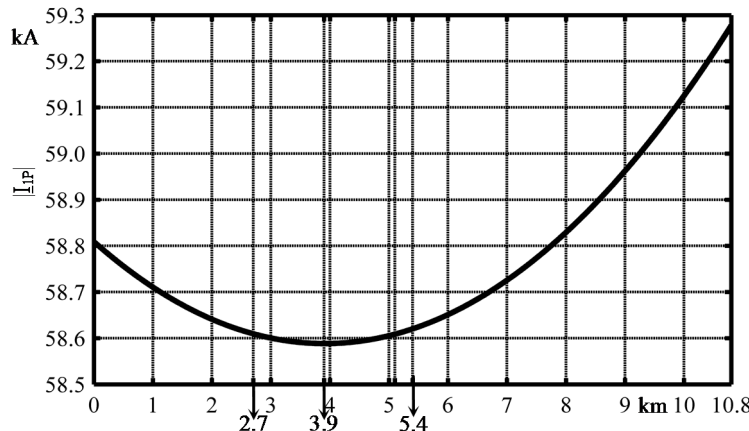
By comparing the aforementioned values with the more accurate ones from the MCA, the following error of sequence approach can be evaluated:

$$\begin{aligned} |I_{IP}|_{MCA} &= 58.604 \text{ kA}; \\ |I_{IP}|_{SI} &= 58.620 \text{ kA}; \end{aligned} \Rightarrow 100 \cdot \frac{|I_{IP}|_{MCA} - |I_{IP}|_{SI}}{|I_{IP}|_{MCA}} = -0.027\%$$

It is extremely low since the UGC CB with PTs is almost symmetric. The error would have been greater if PTs are not performed. The sequence theory can be also used to investigate the point along the line where the lower and higher short circuit current (phase-to-screen fault) occurs. By considering the fault levels, the sequence impedances for each substation can be computed by the well-known formulae shown in [1]; with regard to the UGC impedances, the computation of positive-negative and zero sequence kilometric impedances is explained in detail in [26]. In Figure 18, the phase-to-screen short

circuit current magnitude computed by means of the sequence theory along the line in CB with PTs is shown. The point where the minimum fault current occurs ($|I_{IP}| = 58.588 \text{ kA}$) is at 3.9 km from substation S, whereas the maximum fault current is for a fault at substation R ($|I_{IP}| = 59.278 \text{ kA}$).

Figure 18. Phase-to-screen short circuit current magnitude along line in a single circuit UGC.



The differences between the results obtained by means of sequence theory and MCA are very small. With regard to the double circuit, Table 3 shows the different results by means of MCA and sequence theory by neglecting the mutual zero sequence impedance. The very small differences reported in Table 3 demonstrate that, for UGC, it is licit to neglect the mutual zero sequence impedance due to the great spacing between the two circuits. The scheme to be considered is shown in Figure 19 for the positive and zero sequences respectively.

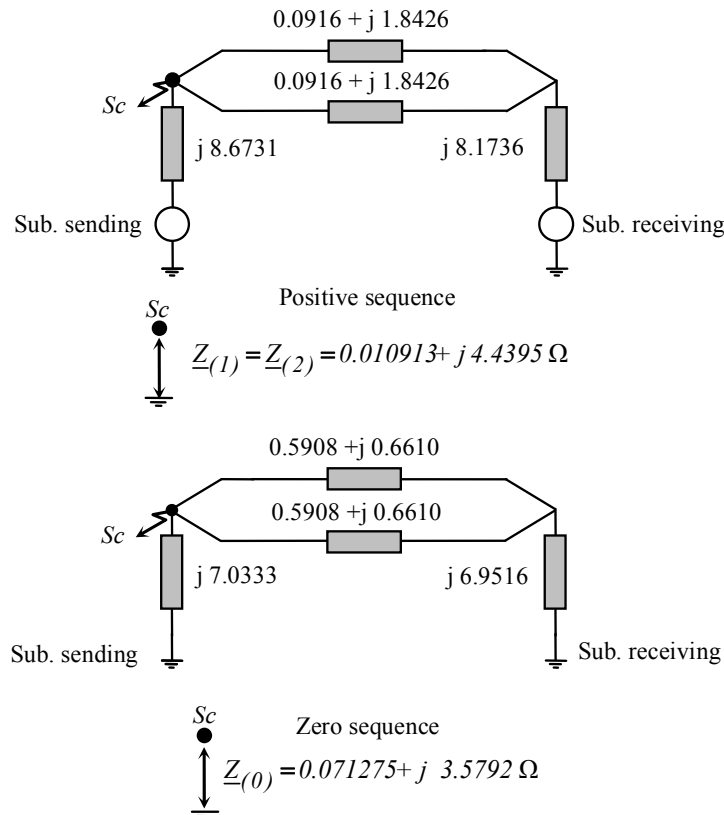
Table 3. Comparison between the MCA and sequence impedances (SI) approach for double circuit UGC.

CB fault location Faulted screen 8 with corresponding phase 2	MCA (kA)	SI (kA)	$100 \cdot \frac{MCA - SI}{MCA} (\%)$
Substation S	61.186	61.171	0.0245
Substation R	61.438	61.436	0.0033
5.4 km from Sub. S	58.619	58.622	-0.0051

The single-phase short circuit current is given by:

$$I_{IP} = \frac{c \cdot 3 \cdot U_0}{\underline{Z}_{(1)} + \underline{Z}_{(2)} + \underline{Z}_{(0)}} = \frac{c \cdot 3 \cdot 400000}{\sqrt{3} \cdot (0.0931 + j \cdot 12.458)} = 61.171 \text{ kA} \angle -89.572^\circ$$

Figure 19. Faulted double circuit UGC: positive and zero sequence circuit for single-phase short circuit at sending-end.



6. Conclusions

The whole ground return current behaviour along UGC (and not only some values at given sites) can be computed by means of MCA. Comparisons with EMTP-RV are fully satisfactory with errors much less than 1%. It is worth highlighting that EMI and AC corrosion possibilities can be evaluated (only) with realistically accurate and safe knowledge of steady-state I_{GR} behaviour. The paper deals with the I_{GR} computation in faulty occurrence but some authors have also shown it in steady-state regimes [7]. The following conclusions can be drawn:

- The steady-state $|I_{GR}|$ for CB with PTs is almost null (not shown in this paper, see [7]) so that, in this aspect, the UGC gives greater guarantees than OHL for ac corrosion issues and electromagnetic interference [7];
- The short circuit $|I_{GR}|$ is significantly influenced by the different values of both the major section CB box resistances and the substation grid ones since the metallic screens are earthed at each major section and at the substation sites: the lower the value of substation grid resistances the lower the magnitude of ground return current;
- The use of sequence impedance approach only for short circuit computations gives slight errors since the transposed UGCs are a rather symmetric system. Of course, the sequence theory approach cannot give $|I_{GR}|$;
- The double-circuit UGC gives (in the same conditions of single-circuit UGC) lower ground return current magnitudes;

- k -factors are valid for solid bonded cables. They are not applicable to cross-bonded UGCs whether single-circuit or a double-circuit;
- IEC 60909-2 and 60909-3 give k -factors only for solid bonded three single-core cables laid in trefoil and flat configurations so that no evaluation is possible for cross-bonded cables which are the usual screen arrangement of HV-EHV cables. IEC k -factor applied to SB cables in flat laying gives an underestimate of about 10%.

Once again, MCA has been compared with EMTP-RV environment with a fully satisfactory agreement. In conclusion the authors hope to have given a powerful tool which allows the reader to implement MCA matrix algorithms, and to know the exact and complete behaviours of UGC screen and phase faulty regimes including ground return current.

Conflicts of Interest

The authors declare no conflicts of interest.

References

1. Benato, R.; Sessa, S.D.; Guglielmi, F. Determination of steady-state and faulty regimes of overhead lines by means of multiconductor cell analysis (MCA). *Energies* **2012**, *5*, 2771–2793.
2. Benato, R.; Paolucci, A. Multiconductor cell analysis of skin effect in Milliken type cables. *Electr. Power Syst. Res.* **2012**, *90*, 99–106.
3. Benato, R.; Forzan, M.; Marelli, M.; Orini, A.; Zaccone, E. Harmonic behaviour of HVDC cables. *Electr. Power Syst. Res.* **2012**, *89*, 215–222.
4. Benato, R.; Caldon, R. Distribution line carrier: Analysis procedure and applications to distributed generation. *IEEE Trans. Power Deliv.* **2007**, *22*, 575–583.
5. Benato, R.; di Mario, C.; Koch, H. High capability applications of long gas insulated lines in structures. *IEEE Trans. Power Deliv.* **2007**, *22*, 619–626.
6. Benato, R.; Caldon, R.; Paolucci, A. Matrix algorithm for the analysis of high speed railway and its supply system. *L'Energ. Elettr.* **1998**, *75*, 304–311. (In Italian)
7. Benato, R. Multiconductor analysis of underground power transmission systems: EHV AC cables. *Electr. Power Syst. Res.* **2009**, *79*, 27–38.
8. Popović, L.M. Determination of the reduction factor for feeding cables consisting of three single-core cables. *IEEE Trans. Power Deliv.* **2003**, *18*, 736–743.
9. Sarajcev, I.; Majstrovic, M.; Sutlovic, E. Influence of earthing conductors on current reduction factor of a distribution cable laid in high resistivity soil. In Proceedings of the 2001 IEEE Power Tech Conference, Porto, Portugal, 10–13 September 2001.
10. Sarajcev, I.; Majstrovic, M.; Sutlovic, E. Determining currents of cable sheaths by means of current load factor and current reduction factor. In Proceedings of the 2003 IEEE Power Tech Conference, Bologna, Italy, 23–26 January 2003.
11. Sarajcev, I.; Majstrovic, M.; Medic, I. Current reduction factor of compensation conductors laid alongside three single-core cables in flat formation. In Proceedings of the 2003 IEEE International Symposium on Electromagnetic Compatibility, Istanbul, Turkey, 11–16 May 2003.

12. Popović, L.M. Practical method for evaluating ground fault current distribution in station, towers and ground wire. *IEEE Trans. Pow. Deliv.* **1998**, *13*, 123–128.
13. Popović, L.M. Efficient reduction of fault current through the grounding grid of substation supplied by cable line. *IEEE Trans. Pow. Deliv.* **2000**, *15*, 556–561.
14. Popović, L.M. Ground fault current distribution in stations supplied by a line composed of a cable and an overhead section. *Eur. Trans. Electr. Power* **2007**, *17*, 207–218.
15. Popović, L.M. Determination of actual reduction factor of HV and MV cable lines passing through urban and suburban areas. *Electron. Energ.* **2014**, *27*, 25–39.
16. Popović, L.M. Ground fault current distribution for the fault anywhere along the feeding line consisting of three single-core cables. In Proceedings of the Sixth International Symposium Nikola Tesla, Belgrade, Serbia, 18–20 October 2006.
17. Popović, L.M. Improved analytical expressions for the reduction factor of feeding lines consisting of three single-core cables. *Eur. Trans. Electr. Power* **2008**, *18*, 190–203.
18. Viel, E.; Griffiths, H. Fault current distribution in HV cable systems. *IEEE Proc. Gener. Transm. Distrib.* **2000**, *147*, 231–238.
19. Viel, E.; Griffiths, H. Determination of ground return currents for earth faults fed by metal sheathed/screened cables. A Case Study. In Proceedings of the 33rd Universities Power Engineering conference, UPEC' 98, Edinburgh, UK, 8–10 September 1998; pp. 715–718.
20. *Short-Circuit Currents in Three-Phase a.c. Systems—Part 2: Data of Electrical Equipment for Short-Circuit Current Calculations*; IEC/TR 60909-2 Ed. 2.0; International Electrotechnical Commission (IEC): Geneva, Switzerland, 2008.
21. *Short-Circuit Currents in Three-Phase a.c. Systems—Part 3: Currents during Two Separate Simultaneous Line-to-Earth Short-Circuits and Partial Short-Circuit Currents Flowing through Earth*; IEC 60909-3 Ed. 2.0; International Electrotechnical Commission (IEC): Geneva, Switzerland, 2003.
22. *Short-Circuit Currents in Three-Phase a.c. Systems—Part 0: Calculation of Currents*; IEC 60909-0 Ed. 1.0; International Electrotechnical Commission (IEC): Geneva, Switzerland, 2001.
23. Sutton, S.; Plath, R.; Schröder, G. The St. Johns wood—elstree experience—testing a 20 km long 400 kV XLPE-insulated cable system after installation. In Proceedings of the 7th International Conference on Insulated Power Cable JiCable07, Versailles, France, 24–28 June 2007.
24. Sadler, S.; Sutton, S.; Memmer, H.; kaumanns, J. 1600 MVA electrical power transmission with an EHV XLPE cable system in the underground of London. In Proceedings of the Cigré 2004, Paris, France, 29 August 2004.
25. Tsuchiya, S.; Iida, T.; Morishita, Y.; Tnkajim, A.; Akiya, Y.; Kurata, T. EHV cable installation technology for tunnels and ducts in Japan. In Proceedings of the Cigré 2012, Paris, France, 26 August 2012.
26. Benato, R.; Caciolli, L. Sequence impedances of insulated cables: Measurements *versus* computations. In Proceedings of the Transmission and Distribution Conference and Exposition (T&D), 2012 IEEE PES, Orlando, FL, USA, 7–10 May 2012.